# A Synthetic Nervous System with Coupled Oscillators Controls Peristaltic Locomotion

Shane Riddle[1(✉)], William R. P. Nourse[2], Zhuojun Yu[3], Peter J. Thomas[2,3], and Roger D. Quinn[1]

[1] Department of Mechanical and Aerospace Engineering, Case Western Reserve University, Cleveland, OH 44106, USA
shane.riddle@case.edu

[2] Department of Electrical, Computer, and Systems Engineering, Case Western Reserve University, Cleveland, OH 44106, USA

[3] Department of Mathematics, Applied Mathematics, and Statistics, Case Western Reserve University, Cleveland, OH 44106, USA

**Abstract.** This paper details the development and analysis of a computational neuroscience model, known as a Synthetic Nervous System, for the control of a simulated worm robot. Using a Synthetic Nervous System controller allows for adaptability of the network with minimal changes to the system. The worm robot kinematics are inspired by earthworm peristalsis which relies on the hydrostatic properties of the worm's body to produce soft-bodied locomotion. In this paper the hydrostatic worm body is approximated as a chain of two dimensional rhombus shaped segments. Each segment has rigid side lengths, joints at the vertices, and a linear actuator to control the segment geometry. The control network is composed of non-spiking neuron and synapse models. It utilizes central pattern generators, coupled via interneurons and sensory feedback, to coordinate segment contractions and produce a peristaltic waveform that propagates down the body of the robot. A direct perturbation Floquet multiplier analysis was performed to analyze the stability of the peristaltic wave's limit cycle.

**Keywords:** Synthetic nervous system · Central pattern generator · Peristalsis · Functional subnetwork · Motor control · Worm robot

## 1 Introduction

Worms move via a process known as peristaltic locomotion, in which the muscles contract and relax in wavelike patterns propagating down the body [16]. The pattern of muscle activation propels the worm forward or backward depending

This work was supported by NSF PIRE Award 1743475, NIH BRAIN Initiative grant R01 NS118606, and NSF DBI 2015317 as part of the NSF/CIHR/DFG/FRQ/UKRI-MRC Next Generation Networks for Neuroscience Program.


A. Hunt et al. (Eds.): Living Machines 2022, LNAI 13548, pp. 249–261, 2022.
https://doi.org/10.1007/978-3-031-20470-8_25

on the direction of the wave, a process made possible by the hydrostatic properties of the worm body. Hydrostats maintain a constant volume due to the incompressibility of fluids within the body. A worm body can be approximated as a series of hydrostatic cylinders known as segments, each of which has longitudinal and circumferential muscles. When the circumferential muscles contract, the segment diameter decreases, which necessitates an increase in length to maintain the volume of the segment. Similarly, contraction of the longitudinal muscles causes a shortening of the segment, which necessitates an expansion of the diameter. Stringing a series of these segments together forms an analogous worm body. Many worm-like robots have been constructed following geometric approximations of this motion [5,8,11].

A Synthetic Nervous System (SNS) is a dynamical network composed of biologically-inspired neuron and synapse models [13]. An SNS can be differentiated from artificial neural networks by its use of conductance-based synapses, rather than weight-based synapses, and the use of the Functional Subnetwork Approach (FSA) [13]. The FSA is a method that allows for direct analytical tuning of small dynamical networks so they may perform specific operations in a larger network without resorting to global optimization methods. These functional subnetworks can be made to perform such actions as addition, subtraction, multiplication, division, differentiation, and integration of incoming signals. The subnetworks can then be assembled to form an SNS for the control of biologically inspired robots [2,5,6,8,14].

The wave-like nature of peristalsis implies periodic behavior in the nervous system. Oscillator networks called central pattern generators (CPGs) are believed to control rhythmic behaviors like breathing, walking, flying, and swimming [9]. CPGs produce periodic outputs without requiring periodic inputs. For peristalsis, CPGs can be used to control the muscle contraction cycles of each segment [7]. This paper develops an SNS neural controller for peristaltic locomotion of a model of a worm-like robot. We hypothesize that coupled oscillators can be used to produce peristaltic waveforms for use in worm-like locomotion.

## 2 Simplified Worm Robot Kinematic Model

For the purposes of this work, the worm robot segment model is simplified using rhombuses with hinge joint vertices [8]. This model operates similarly to the hydrostat cylinder model but in two dimensions instead of three. The worm body segments consist of rhombuses linked corner to corner with joints at all vertices. It is assumed that the sides of these rhombuses are rigid and that the angle between adjacent sides can change via joints placed at each vertex. Pushing two opposing corners together results in an outward displacement of the other two corners in the rhombus (Fig. 1a). This is akin to the hydrostat longitudinal contraction. Pulling the other two corners together similarly displaces the first pair of vertices (Fig. 1b). This is akin to the hydrostat circumferential contraction. Just as in the hydrostat model these are antagonistic actions that can propagate down a worm body in a peristaltic wave. The relationship between rhombus height ($w$) and length ($l$) for a given side length ($l_s$) is $l^2 + w^2 = 4l_s^2$.

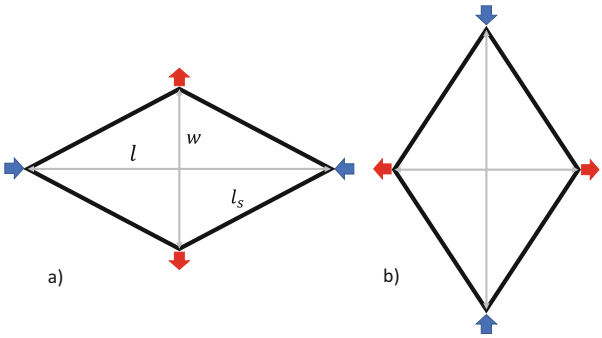


**Fig. 1.** Rhombus segment at two states: a) fully contracted and expanding, b) fully expanded and contracting.

The robot discussed in this paper is simulated but was loosely modelled after an existing robot presented in [4]. The physical robot uses servo motors connected to cords wrapped around the circumference of a cylinder composed of flexible rhombuses. For a visual of this robot, refer to Fig. 3 of [4]. Spooling and unwinding the cord directly changes the heights of the rhombuses resulting in segment contraction and expansion, respectively. While the motor is only able to provide contracting tension to the cord, longitudinally oriented springs provide return force allowing for control of both directions of movement. The simulation in this work models the motors as linear actuators. Each rhombus segment has one such actuator spanning between its top and bottom vertices.

These motors use proportional control, whereby the actuator velocity ($v$) is determined by the difference between the current height ($w_i$) and target height ($w_{\text{targ}}$). The subscript $i$ indicates the simulation time step and $w_{\text{targ}}$ is set by the CPG neurons as detailed in Sect. 3.1. The equation governing the actuator velocity is $v = k * (w_{\text{targ}} - w_i)$, where $k$ is a gain that can be tuned to achieve a desired actuation behavior. For the purposes of this paper $k$ was set to 0.0091. The height updates at each time step (of size $dt$) following the equation $w_i = w_{i-1} + v * dt$. The velocity also updates so the actuation speed decreases as the segment height approaches $w_{\text{targ}}$. The segment length is calculated at each time step via the geometric relationship $l_i = \sqrt{4l_s^2 - w_i^2}$. Maximum and minimum height limits ($w_{\max} = 11\text{cm}$, $w_{\min} = 6.5\text{cm}$) were set to reflect the physical limits of the robot in [4], however the limits are arbitrary so long as they do not violate the geometry. At these limits the actuator velocity is set to zero.

## 3 Methods

### 3.1 Mathematical Models

**Neurons and Synapses:** As stated previously, the SNS is composed of neurons and synapses. Non-spiking, leaky integrator neurons were chosen for this network. The leaky-integrator dynamics convey ion channel gating without expressing action potentials generated by Hodgkin-Huxley (H-H) fast transient sodium

and delayed rectifier potassium currents [3,13]. Omitting action potentials simplifies the neuron model by removing the non-linear differential equations needed to properly convey H-H ion channel gating. The activity of this type of neuron is qualitatively comparable to the spiking frequency of a population of spiking neurons, whereby increasing spiking frequency in the population correlates to increasing membrane potential in the non-spiking neuron [15,18]. The simpler equations and ability to model one neuron instead of a population leads to a more computationally efficient controller. This is essential for robotic applications as the controllers must be capable of real-time operation for practical use. The differential equation governing the membrane potential behavior of the non-spiking neuron model is as follows:

$$C_m \frac{dV}{dt} = G_m(E_r - V) + \sum_{j=1}^{n} G_{\text{syn},j}(E_{\text{syn},j} - V) + I_{\text{app}} \tag{1}$$

$C_m$ is the membrane capacitance, $V$ is the membrane potential, $G_m$ is the membrane conductance, and $E_r$ is the cell's resting potential. $E_{\text{syn}}$ is the synaptic reversal potential, $n$ is the number of presynaptic neurons, and $I_{\text{app}}$ is any current applied directly to the neuron. $G_{\text{syn}}$ is the synaptic conductance through which presynaptic neuron $j$ influences the postsynaptic neuron. Non-spiking conductance-based synapses were chosen for this network [13]. These are synapses which only influence the post-synaptic neuron if the presynaptic neuron is excited. Unlike the leak term ($G_m$) the synaptic conductance depends on the presynaptic neuron potential. In biological models this relationship, known as the synaptic conductance curve, can be represented by any monotonic function that saturates, like a sigmoid. For this SNS a piecewise linear approximation is used [13]. This allows for precise tuning of the network (shown in Sect. 3.2) and reduces the complexity of the math involved. The synaptic conductance curve is defined by the following:

$$G_{\text{syn},i} = \begin{cases} 0 & \text{when } V_{\text{pre}} < E_{\text{lo}} \\ g_{\text{syn},i} \dfrac{V_{\text{pre}} - E_{\text{lo}}}{E_{\text{hi}} - E_{\text{lo}}} & \text{when } E_{\text{lo}} \leq V_{\text{pre}} \leq E_{\text{hi}} \\ g_{\text{syn},i} & \text{when } V_{\text{pre}} > E_{\text{hi}} \end{cases} \tag{2}$$

$E_{\text{hi}}$ and $E_{\text{lo}}$ are the upper and lower threshold potentials of the synapse and their difference is known as the "operating range" $R$ ($R = E_{\text{hi}} - E_{\text{lo}}$). From Eq. 2 we can see that this means the synapse is essentially off when $E_{\text{lo}}$ is reached and saturates at its maximum conductance ($g_{\text{syn}}$) when $E_{\text{hi}}$ is reached. To simplify this equation the actual membrane potential of the cell is normalized to be 0mV at rest. The normalized potential is represented by the variable $U$ which is the neuron activation level above resting potential ($U = V - E_r$). Assuming the synaptic potentials stay within the operating range $(0, R)$ we can substitute $U$ and $R$ into Eq. 2 to reduce the piecewise linear relationship to just $g_{\text{syn},i} \frac{U_{\text{pre}}}{R}$. Since the membrane potential was normalized to $U$, the synaptic

reversal potential must also be corrected ($\Delta E_{\text{syn}} = E_{\text{syn}} - E_r$). Substituting these parameters into Eq. 1 produces the following:

$$C_m \frac{dU}{dt} = -G_m U + \sum_{j=1}^{n} g_{\text{syn},j} \frac{U}{R}(E_{\text{syn},j} - U) + I_{\text{app}} \tag{3}$$

This ordinary differential equation can be solved using the forward Euler numerical method of approximation. In this method the time differential components are calculated at each time step $i$ and build off the state of the neuron at the previous time step $i-1$. When converted into this format and solved for U, the differential equation takes the following form:

$$U_i = U_{i-1} + \frac{dt}{C_m}(-G_m U_{i-1} + \sum_{j=1}^{n} g_{\text{syn},j} \frac{U_{i-1}}{R}(E_{\text{syn},j} - U_{i-1}) + I_{\text{app}}) \tag{4}$$

**Central Pattern Generators:** The driving components of the SNS controller are the CPGs [10,12]. Each segment has one CPG composed of two neurons: one encouraging segment contraction ($U_1$), the other segment expansion ($U_2$). The activation levels of the CPG neurons directly control the actuator's target position. The target position is set by subtracting the membrane potential of the contracting neuron from that of the expanding neuron. Each CPG neuron's operating range is between 0 and $R$, meaning the total range of values for this operation is $[-R, R]$. This range is mapped to the range of heights the segments are capable of achieving $[w_{\min}, w_{\max}]$. When the contraction neuron is more strongly activated the actuator decreases the segment height (not exceeding $w_{\min}$). When the expansion neuron is more strongly activated the segment height increases (not exceeding $w_{\max}$).

The CPG neurons use the same non-spiking model but now incorporate voltage-gated sodium ion channels [12]. This allows for additional temporal dynamics that enable pattern generation. The ion channels are modeled using fast m gates and slow h gates, like those in the H-H model [3]. The m and h gating variable behaviors are modeled using the following functions:

$$h_\infty(U) = \frac{1}{1 + 0.5e^{s_h * (U)}} \tag{5}$$

$$m_\infty(U) = \frac{1}{1 + e^{s_m * (U-R)}} \tag{6}$$

$$\tau_h(U)\frac{dh}{dt} = h_\infty(U) - h \;\longrightarrow\; \tau_h(U) = \tau_{h,\max}\frac{\sqrt{0.5e^{s_h*(U)}}}{h_\infty(U)} \tag{7}$$

The $s$ values are the slopes of the sigmoids dictating the behaviors of $m$ and $h$ while $\tau_h$ is the time constant that determines how fast the h gates close. The m gates are much faster than the h gates which means $\tau_m$ is significantly smaller than $\tau_h$. This allows us to ignore $\tau_m$.

The sodium channel current presents as $G_{\text{Na}} m_\infty(U) h(U) * (\Delta E_{\text{Na}} - U)$ in the neuron model. $G_{\text{Na}}$ is the sodium conductance that allows the $U_1$ CPG neuron's

steady state potential to be $R$ at equilibrium when the other neuron's potential $U_2$ is at 0. Analyzing the sodium conductance in this state lets us find $G_{\text{Na}}$ using the following calculation instead of solving a four-dimensional system.

$$G_{\text{Na}} = \frac{G_m R}{m_\infty(R) h_\infty(R) * (\Delta E_{\text{Na}} - R)} \tag{8}$$

The CPG structure is composed of two of these neurons mutually inhibiting each other, known as the half-center model [1]. The mutual inhibition paired with the sodium channel behavior allows the neurons to switch back and forth between excited and inhibited states in a catch-and-release fashion. When the excited neuron's potential drops below the necessary threshold the inhibition of the other neuron lets up just enough for the fast m gates to start opening. This results in the cascading effect which quickly depolarizes the neuron and simultaneously inhibits/ hyperpolarizes the previously excited neuron. This cycle continues indefinitely unless halted by an outside force such as an applied current.

**Sensors:** Each segment is equipped with a stretch sensor oriented longitudinally between the middle vertices of the rhombus (see Fig. 3 of [4]). The signal from the stretch sensor is approximated as a piecewise function such that it sends a current directly to the CPG command neuron ($U_3$ of the SNS diagram in Fig. 2) only when the segment reaches its minimum length/maximum height (fully expanded state). This function is shown below.

$$I_{\text{sens}} = \begin{cases} R & \text{when } l \leq l_{\min} \\ 0 & \text{when } l \geq l_{\min} \end{cases} \tag{9}$$

The applied current value of $R$ was chosen to keep the math simple when tuning the network.

### 3.2 Functional Subnetwork Tuning

The worm robot's Synthetic Nervous System (Fig. 2) was developed using the neuroscientific models described in Sect. 3.1. The SNS is split up into subnetworks corresponding to the "physical" worm segments. As such there are $N$ CPGs, stretch sensors, command neurons ($U_3$), and inter-segment neurons ($U_4$) where $N$ is the number of worm segments in the model (any integer of value 3 or greater works for peristalsis). The order of operations within each segment is broken down in the flowchart in Fig. 3. Each synapse is tuned by taking the parameter values of the relevant pre and postsynaptic neurons at a given point in the cycle outlined in the flowchart and applying these to the following equation (where $n$ signifies the number of presynaptic neurons influencing the postsynaptic neuron).

$$U^* = \frac{\sum_{j=1}^{n} g_{\text{syn},j} \frac{U_{j,\text{pre}}}{R} E_{\text{syn},j} + I_{\text{app}}}{G_m + \sum_{j=1}^{n} g_{\text{syn},j} \frac{U_{j,\text{pre}}}{R}} \tag{10}$$

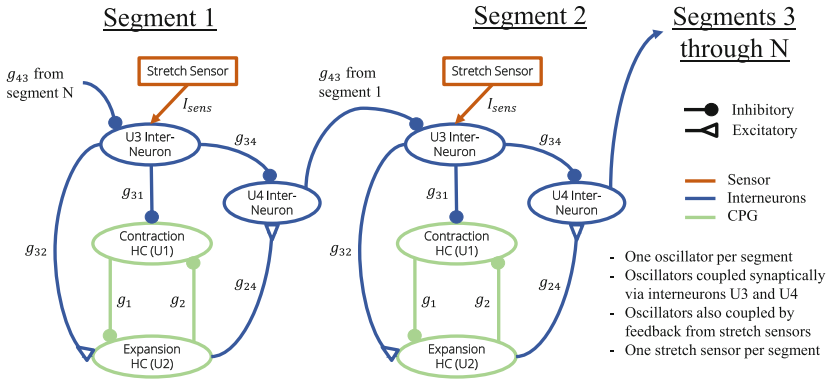


**Fig. 2.** Synthetic Nervous System controller diagram for a simulated worm robot

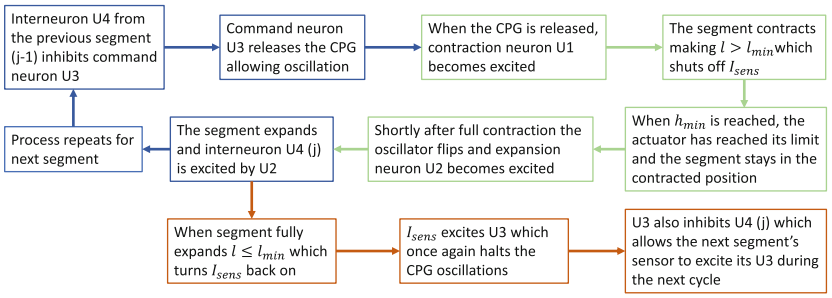


**Fig. 3.** Flowchart explaining the SNS diagram operations in order

This equation is the key for direct analytical tuning of transmission synapses via the FSA as presented in [13]. $U^*$ here is the desired steady state potential of the postsynaptic neuron for a given set of presynaptic potentials. For this network $G_m = 1\,\mu$S, $C_m = 5\,$nF, $E_r = -60\,$mV, and $R = 20\,$mV or nA depending on the parameter. All inhibitory synaptic reversal potentials ($E_{\text{inh}}$) were taken to be $-100\,$mV. All excitatory reversal potentials ($E_{\text{ex}}$) were taken to be $134\,$mV, the reversal potential of an excitatory calcium neurotransmitter found in some organisms [13]. Relevant earthworm nervous system data was not readily available to use for this SNS. As such these parameters were chosen somewhat arbitrarily but all values were kept within the realm of biological plausibility (mV, nA, and $\mu$S scales) and follow the guidelines laid out in [13].

The tuning of the synapse between neurons $U_{4,j-1}$ and $U_{3,j}$ ($g_{\text{syn43}}$) will be used to demonstrate the design process. This synapse will be evaluated when $U_{4,j-1}$ is inhibiting $U_{3,j}$ while the sensor is still providing current (just before the CPG restarts). At this point in time $U^*_{3,j} = 0\,$mV since it is inhibited, $I_{\text{sens}} = R = 20$nA since the segment has not yet contracted, and $U_{4,j-1} = R = 20\,$mV since it is excited. When plugged into Eq. 10, the only remaining unknown is $g_{\text{syn43}}$ which can now be solved for:

$$U^*_{3,j} = 0 = \frac{g_{\text{syn43}} \dfrac{U_{4,j-1}}{R} \Delta E_{\text{syn43}} + I_{\text{sens}}}{1 + g_{\text{syn43}} \dfrac{U_{4,j-1}}{R}} = \frac{g_{\text{syn43}} \Delta E_{\text{inh}} + R}{1 + g_{\text{syn43}}}$$
$$\longrightarrow g_{\text{syn43}} = \frac{-R}{\Delta E_{\text{inh}}} = \frac{-20\text{nA}}{-100\text{mV} - (-60\text{mV})} = 0.5\mu\text{S} \tag{11}$$

This process need only be repeated for each of the synapses in a single segment since the parameters are the same for every segment. This $g_{\text{syn}}$ value indicates the maximum conductance parameter to be used in the synapse model in Eq. 2. Finding $g_{\text{syn}}$ constitutes tuning the synapse.

The tuning process for the CPG synapses ($g_{\text{syn1}}$, $g_{\text{syn2}}$) is similar but with one caveat. The CPG neurons have sodium currents and must be able to inhibit each other in such a way that allows their membrane potentials to oscillate back and forth. Since transmission type synapses are used, the synaptic conductance must be designed to make the inhibited neuron's potential ($U_2$) greater than 0 for it to inhibit the excited neuron ($U_1 = R = 20\,\text{mV}$). This value of $U_2$ is denoted by $\delta$, a bifurcation parameter explained in [12]. Substituting delta and the persistent sodium current into Eq. 10 produces the following equation which can then be solved for the maximum synaptic conductance $g_{\text{syn}}$. Note that $g_{\text{syn1}} = g_{\text{syn2}} = g_{\text{syn}}$ for the CPG synapses.

$$\delta = \frac{g_{\text{syn}} \dfrac{U_1}{R} \Delta E_{\text{syn}} + G_{\text{Na}} m_\infty(\delta) h_\infty(\delta) * (\Delta E_{\text{Na}})}{1 + g_{\text{syn}} \dfrac{U_1}{R} + G_{\text{Na}} m_\infty(\delta) h_\infty(\delta)}$$
$$\longrightarrow g_{\text{syn}} = \frac{-\delta - G_{\text{Na}} m_\infty(\delta) h_\infty(\delta)(\delta - \Delta E_{\text{Na}})}{\delta - \Delta E_{\text{Na}}} \tag{12}$$

$E_{\text{Na}}$ was set to 50 mV, a typical value for the sodium reversal potential in a neuron, and $\Delta E_{\text{Na}} = E_{\text{Na}} - E_r$. Other parameter values used for these calculations were $\tau_{h,\max} = 300\,\text{ms}$, $s = 0.05$, and $\delta = 0.01$. Using these parameters to tune the CPG synapses results in a continuous pattern of oscillation between the neuron potentials $U_1$ and $U_2$.

Since the CPG relies on the neuron potentials just barely crossing their thresholds to induce oscillation, it is possible to halt the CPG by applying current to the neurons. This can be done directly or through a synaptic connection from a command neuron. By exciting the expansion CPG neuron while it is already excited, and inhibiting the contraction CPG neuron when it is inhibited, the command neuron ($U_3$) is able to push their potentials away from the thresholds thus halting oscillation. When the command neuron is inhibited this influence is released allowing oscillation to resume.

### 3.3 Stability Analysis

For the parameters used in this work, the simulated robot with $N = 6$ segments exhibits a stable limit cycle with a period $T \approx 5250\text{ms}$. That is, there is a

unique periodic orbit that attracts nearby trajectories. In order to confirm the stability of the orbit we performed a direct Floquet multiplier analysis as follows. There are seven variables per segment: four neuron potentials, two "h" gating variables, and the segment height. Thus there are 42 variables for a robot with six segments. Given a base point $\mathbf{x}_0 \in \mathbb{R}^{42}$, we consider 42 different trajectories with perturbed initial conditions $\mathbf{x}_i(0) = \mathbf{x}_0 + \epsilon\,\mathbf{e}_i$, where $\mathbf{e}_i \in \mathbb{R}^{42}$ is the $i$th standard unit vector, and $|\epsilon| \ll 1$. We construct an approximation to the Monodromy matrix $M$, defined with the $i$th column $M_i$ given by

$$M_i = \lim_{\epsilon \to 0} \frac{\mathbf{x}_i(T) - \mathbf{x}_0}{\epsilon},$$

where $\mathbf{x}_i(T)$ is the point on the perturbed trajectory after one period evolution. The periodic orbit is linearly stable if and only if the eigenvalues of $M$, the Floquet multipliers, may be ordered such that

$$\lambda_1 \equiv 1 > |\Re(\lambda_2)| \geq |\Re(\lambda_3)| \geq \ldots \geq |\Re(\lambda_{42})|.$$

The Monodromy matrix $M$ obtained depends on the choice of base point $\mathbf{x}_0$; in theory the eigenvalues of $M$ are independent of $\mathbf{x}_0$. For the specific base point used here, see the code available at https://github.com/sriddle97/SNS-Controlled-Peristalsis.git.

## 4 Results

### 4.1 SNS Simulation

Running the simulation with all the parameters set, neurons modelled, and synapses tuned as described in Sect. 3 produced the results in Fig. 4. $N$ was chosen to be 3 for these plots for the purposes of legibility. $N = 6$ was still used for the stability analysis.

Figure 4 shows that the SNS network does induce sequential CPG activity from segment to segment down the worm body. As intended, the CPGs halt when their sensor detects full re-expansion of the segment thus applying current to the command neuron $U_3$ which inhibits $U_1$ and excites $U_2$. The CPG begins oscillating once more when the previous segment's $U_4$ neuron inhibits the $U_3$ command neuron, thus removing its effect on the CPG. In this way the CPGs are effectively coupled via the $U_4$ inter-segment neuron and the stretch sensors. The height plots in Fig. 4 show that this coupling allows the propagation of a peristaltic waveform when the CPG potentials are mapped to the actuator model to produce segment motion. Close inspection of the neuron potential and height plots reveals that the segment height decreases when it's corresponding CPG neuron $U_1$ is excited. This makes sense since $U_1$ encourages segment contraction. Likewise, when the expansion CPG neuron $U_2$ is excited, the segment height increases. Since $U_2$ excites the inter-segment neuron $U_4$ which then starts the oscillation of the following segment, the wave is able to propagate down the worm from segment to segment in a peristaltic fashion.

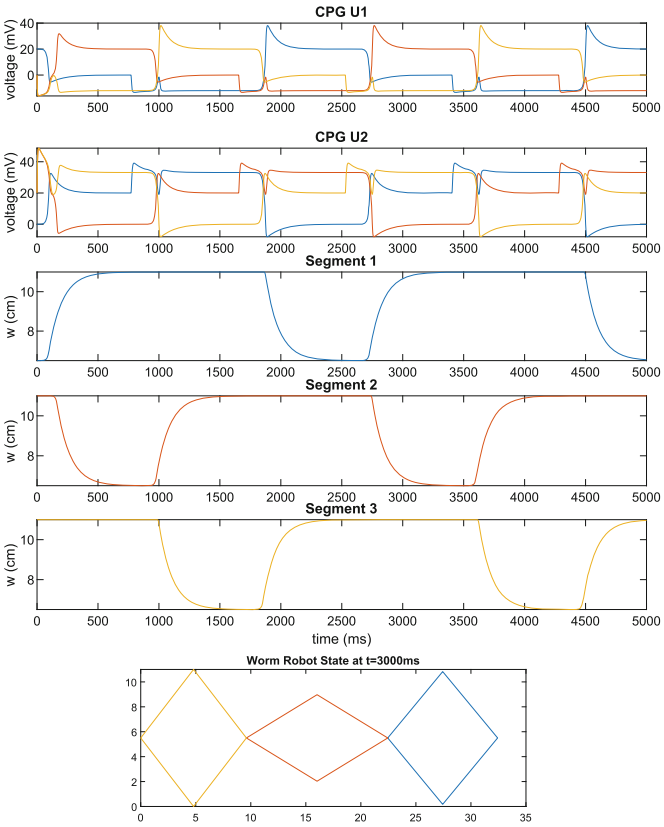


**Fig. 4.** Plot of the CPG neuron membrane potentials and segment heights over time, as well as a snapshot of the simulation at t=3000 ms, color coded by segment. (Color figure online)

### 4.2 Stability

We obtained the Monodromy matrix $M$ via direct estimation, using a perturbation of $\epsilon = 0.001$. When a height variable is on the upper threshold $h = h_{\max}$, linear disturbances are automatically rejected. Thus, linear order, small perturbations in the height lead to no perturbation of the limit cycle when the perturbed variable is pressed against a hard boundary. That is, the system has a limit cycle with a sliding component [17]. The corresponding columns of $M$ are thus identically equal to zero, meaning that if $j$ variables are thus constrained at the reference point $\mathbf{x}_0$ anchoring the Floquet analysis, the $42 \times 42$ matrix $M$ necessarily has rank $\leq 42 - j$. Consequently at least $j$ of the multipliers are identically zero, indicating the presence of "superstable" directions at $\mathbf{x}_0$. Using the direct analysis, we obtained that the leading Floquet multipliers are

$$\lambda_1 = 0.9945 \approx 1, \quad \lambda_2 = 0.0081, \quad \lambda_3 = -0.0001,$$

and the remaining multipliers are either identically zero or else negligibly small. The nontrivial Floquet multipliers are less than 1 in magnitude, indicating that the periodic orbit of our model is linearly stable. For the full Monodromy matrix and list of Floquet multipliers see the code linked in Sect. 3.3.

## 5 Discussion and Future Work

We hypothesized that coupled oscillators can form peristaltic waves in a worm robot model. The results in Sect. 4 indicate that it is indeed possible, thus confirming the hypothesis. The CPGs coupled via the inter-segment neurons $U_4$ and the stretch sensors are capable of propagating a signal from segment to segment. The CPGs themselves are also effective in controlling the pattern of segment contraction and expansion that translates this signal into peristaltic locomotion. Thus, the SNS described in this paper is capable of controlling a simple worm-like robot model. Direct evaluation of the Floquet multipliers for the periodic orbit suggested that the periodic motions of the neural and mechanical elements together indeed produce a linearly stable limit cycle.

While the simple worm-robot model described in this paper could be controlled via a state machine or conventional artificial neural network (ANN), the SNS controller has advantages. Adding complexity to the mechanical model to make it more realistic may require a full re-design of a state machine controller. An SNS may only require a few additional neurons or a subnetwork to account for the changes [10,13]. Additionally, SNSs do not require large amounts of computational power or training data for global optimization methods (such as genetic algorithms) unlike ANNs [13]. The direct analytical tuning of an SNS also makes it tractable unlike the black box controllers produced by global optimization.

In its present state the kinematic model does not sufficiently capture the detailed movements of a physical robot. As such, both the model and the SNS controller designed in this paper need alteration before use in a real-world context. Most of this alteration could be accomplished by re-designing the model to include forces and compliant mechanical coupling between segments, making it a kinetic model. This would allow the application of friction force which must be accounted for to mitigate segment slip and to accurately portray contact with the robot's environment [4]. Incorporating a more complex motor controller would also allow the motors to have a wider range of actuation patterns/behaviors which could enable more efficient locomotion [8]. Lastly, more research on earthworm nervous systems could be performed. Some parts of the SNS structure, like the back-to-front synaptic connection between segment N and segment 1, were included to make the system functional but are not necessarily features grounded in neuroscience literature. Further study could reveal neural architectures and properties that could be used to make the SNS even more biologically relevant.

## References


1. Brown, T.G.: On the nature of the fundamental activity of the nervous centres; together with an analysis of the conditioning of rhythmic activity in progression, and a theory of the evolution of function in the nervous system. J. Physiol. **48**(1), 18–46 (1914)
2. Goldsmith, C.A., Szczecinski, N.S., Quinn, R.D.: Neurodynamic modeling of the fruit fly drosophila melanogaster. Bioinspiration Biomimetics **15**(6), 065003 (2020)
3. Hodgkin, A.L., Huxley, A.F.: A quantitative description of membrane current and its application to conduction and excitation in nerve. J. Physiol. **117**(4), 500–544 (1952)
4. Horchler, A.D., et al.: Peristaltic locomotion of a modular mesh-based worm robot: Precision, compliance, and friction. Soft Rob. **2**(4), 135–145 (2015)
5. Huang, Y., Kandhari, A., Chiel, H.J., Quinn, R.D., Daltorio, K.A.: Mathematical modeling to improve control of mesh body for peristaltic locomotion. In: Mangan, M., Cutkosky, M., Mura, A., Verschure, P.F.M.J., Prescott, T., Lepora, N. (eds.) Living Machines 2017. LNCS (LNAI), vol. 10384, pp. 193–203. Springer, Cham (2017). https://doi.org/10.1007/978-3-319-63537-8_17
6. Hunt, A., Szczecinski, N., Quinn, R.: Development and training of a neural controller for hind leg walking in a dog robot. Front. Neurorobot. **11**, 18 (2017)
7. Ijspeert, A.J.: Central pattern generators for locomotion control in animals and robots: a review. Neural Netw. Robot. Neurosci. **21**(4), 642–653 (2008)
8. Kandhari, A., Wang, Y., Chiel, H.J., Quinn, R.D., Daltorio, K.A.: An analysis of peristaltic locomotion for maximizing velocity or minimizing cost of transport of earthworm-like robots. Soft Rob. **8**(4), 485–505 (2021)
9. Marder, E., Bucher, D.: Central pattern generators and the control of rhythmic movements. Curr. Biol. **11**(23), 986–996 (2001)
10. Nourse, W., Quinn, R.D., Szczecinski, N.S.: An adaptive frequency central pattern generator for synthetic nervous systems. In: Vouloutsi, V., Halloy, J., Mura, A., Mangan, M., Lepora, N., Prescott, T.J., Verschure, P.F.M.J. (eds.) Living Machines 2018. LNCS (LNAI), vol. 10928, pp. 361–364. Springer, Cham (2018). https://doi.org/10.1007/978-3-319-95972-6_38
11. Seok, S., Onal, C.D., Cho, K.J., Wood, R.J., Rus, D., Kim, S.: Meshworm: Aa peristaltic soft robot with antagonistic nickel titanium coil actuators. IEEE/ASME Trans. Mechatron. **18**(5), 1485–1497 (2013)
12. Szczecinski, N.S., Hunt, A.J., Quinn, R.D.: Design process and tools for dynamic neuromechanical models and robot controllers. Biol. Cybern. **111**(1), 105–127 (2017). https://doi.org/10.1007/s00422-017-0711-4
13. Szczecinski, N.S., Hunt, A.J., Quinn, R.D.: A functional subnetwork approach to designing synthetic nervous systems that control legged robot locomotion. Front. Neurorobot. **11**, 37 (2017)
14. Szczecinski, N.S., Quinn, R.D.: Template for the neural control of directed stepping generalized to all legs of MantisBot. Bioinspiration Biomimetics **12**(4), 045001 (2017)
15. Szczecinski, N.S., Quinn, R.D., Hunt, A.J.: Extending the functional subnetwork approach to a generalized linear integrate-and-fire neuron model. Front. Neurorobot. **14**, 577804 (2020)
16. Tanaka, Y., Ito, K., Nakagaki, T., Kobayashi, R.: Mechanics of peristaltic locomotion and role of anchoring. J. R. Soc. Interface **9**(67), 222–233 (2012)

17. Wang, Y., Gill, J.P., Chiel, H.J., Thomas, P.J.: Shape versus timing: linear responses of a limit cycle with hard boundaries under instantaneous and static perturbation. SIAM J. Appl. Dyn. Syst. **20**(2), 701–744 (2021)
18. Wilson, H.R., Cowan, J.D.: Excitatory and inhibitory interactions in localized populations of model neurons. Biophys. J . **12**(1), 1–24 (1972)